Dispersion of artificial tracers in ventilated caves

Claudio Pastore [1,2*], Eric Weber [1], Frédéric Doumenc [3,4], Pierre-Yves Jeannin [1], and Marc Luetscher [1]

[1]Swiss Institute for Speleology and Karst Studies (SISKA), Rue de la Serre 68, 2300 La Chaux-de-Fonds, Switzerland
[2]Université de Neuchâtel, Avenue du 1er-Mars 26, 2000 Neuchâtel, Switzerland
[3]Université Paris-Saclay, CNRS, FAST, Rue A. Rivière, Bâtiment Pascal (bât. 530), 91405 Orsay Cedex, France
[3]Sorbonne Université, UFR 919, 4 place Jussieu, F-75252 Paris Cedex 05, France

Abstract: Artificial CO_2 was used as a tracer along ventilated karst conduits to infer airflow and investigate tracer dispersion. In the karst vadose zone, cave ventilation is an efficient mode of transport for heat, gases and aerosols and thus drives the spatial distribution of airborne particles. Modelling this airborne transport requires geometrical and physical parameters of the conduit system, including the cross-sectional areas, the airflow and average air speed, as well as the longitudinal dispersion coefficient which describes the spreading of a solute. Four gauging tests were carried out in one mine (artificial conduit) and two ventilated caves (natural conduits). In this paper, we demonstrate that it is possible to gain reliable airflow rates and geometric information of ventilated karst conduits using CO_2 as a tracer. Airflow was gauged along two caves and one mine and compared with punctual measurements made with a hot-wire anemometer. Cross-sectional areas estimated with CO_2 tests were compared with those measured *in situ*. Moreover, breakthrough curve (BTC) analysis displayed an accentuated tailing along the investigated natural conduits due to the presence of dispersive singularities which possibly enable aerosol deposition. The long tailing observed in Milandre and Longeaigue caves is probably due to cross-section variations. A 1-D advection-dispersion model tested for these sites was unable to fit BTC tailing in natural conduits. In Baulmes artificial conduit, where long tailing is not observed, the dispersion coefficient has been estimated using Chatwin's method, and compared with the prediction of Taylor's theory. Despite the regular geometry of Baulmes Mine, Taylor's correlation significantly underestimates the dispersion coefficient deduced from field data, showing the need for more theoretical work on turbulent dispersion in mines. This paper gives a first insight into air motion and matter dispersion along ventilated karst conduits, preparing for proper aerosol dispersion modelling.

Keywords: karst ventilation, chimney effect, airflow, CO_2, tracing test

Received 16 February 2024; Revised 6 April 2024; Accepted 8 April 2024

INTRODUCTION

In the karst vadose zone, cave ventilation is an efficient mode of transport for heat, gases and aerosols and thus drives the spatial distribution of airborne particles (Pashchenko et al., 1993; Christoforou et al., 1994; Dredge et al., 2013; Faimon et al., 2019). Modelling this airborne transport requires geometrical and physical parameters of the conduit system, including the cross-sectional areas, the airflow and average air speed, as well as the dispersion processes which describe the spreading of the transported substance (Hart et al., 2013; Addesso et al., 2022). Geometrical parameters and air velocity can sometimes be measured in the field, but inaccuracies derive from spot measurements which may poorly reflect the average air velocity along the conduits. The sizing of cross-sections is also subject to approximations when extracted from a cave survey. Hence, a method that may provide information about the conduit geometry in a safe, inexpensive, and reliable way would be welcome (Field, 1999, 2002; Hauns, 1999; Palmer et al., 1999; Hauns et al., 2001; Massei et al., 2006). The gauging of air has been extensively used in mine engineering to infer dust and contaminant transport in time and space along the channels to prevent mine operators' health from the release of mine smoke and fumes (Higgins and Shuttleworth, 1958; Thirnonsl & Kissel, 1974; Standish, 1988; Widodo et al., 2008; Widiatmojo et al., 2015; Semin et al., 2022). However, it was only rarely applied to air dynamics in natural cave systems which differ from mines because of

*claudio.pastore@isska.ch

their more complex morphologies. Nevertheless, the dust present in mines is analogous to the airborne aerosols present in caves and includes both, external and internal aerosol sources, anthropogenic (visitors) production, hydrological sources and bedrock production (Dredge et al., 2013). Since the production sources are widely different, the size of particles also varies. The grain dimensions together with the airflow magnitude and flow patterns will control the mode and speed of deposition (Christoforou et al., 1996; Dredge et al., 2013). For instance, the deposition of coarse particles (size > 1 μm) occurs mainly at the cave entrance, whereas fine particles (size < 1 μm) may travel further into the cave.

When a solute is injected in a stream of liquid flowing in a pipe, the interaction between velocity variation over the cross-section and radial diffusion of the solute results in solute dispersion. The solute transport can be described by a 1-D advection-dispersion equation where the dispersion coefficient D (i.e., the effective "diffusion" coefficient in the longitudinal direction) depends on flow characteristics and can be much larger than the thermodynamic diffusion coefficient. Experimental values of D can be obtained from the analysis of breakthrough curves (BTC), i.e., time variations of the solute concentration at a certain distance from the injection point. Taylor (1954) used a method based on the frozen-cloud approximation to extract D from BTC. Chatwin (1971) showed the limits of this assumption and proposed an alternative method based on the linear representation of the two BTC limbs. Furthermore, Taylor (1954) derived a theoretical expression of the dispersion coefficient for a turbulent flow in a rough pipe with a circular cross-section. Based on the empirical velocity profile coupled to the Reynolds analogy to obtain the eddy diffusivity, Taylor's theory states that the dispersion coefficient is simply proportional to the pipe diameter d and the friction velocity U^*, with $D/d \cdot U^* = 5.05$.

Standish (1988) used acetylene (C_2H_2), which has similar physical characteristics (density, molecular weight and diffusivity) to those of air, to infer the dispersion by applying Taylor's method to different injections into ventilated mine tunnels. More recent applications (Widodo et al., 2008; Sasaki et al., 2009; Widiatmojo et al., 2015;) relied on the injection of SF_6 into ventilation conduits to assess the dispersion coefficient solving the 1-D advection-dispersion equation. Their results have clearly shown that, in their case, the ratio $D/d \cdot U^*$ was between 16.5 and 65.5 times higher than Taylor's proportionality coefficient of 5.05. Taylor's approach (Taylor, 1954), which is limited to fully developed flow in a pipe with a circular cross-section, fails to consider singularities as bends, rock blocks and narrow passages. However, these singularities are nonetheless common in natural environments such as caves where their presence needs to be taken into account when trying to assess the dispersion coefficient. The comparison between measured and theoretical BTCs may reveal discrepancies associated with tailing. In hydrogeology and mining aerology, the tailing is interpreted as the effect of singularities (e.g.,

changes in geometries, presence of cavities or solute absorption) on the contaminant transport caused by particles momentarily trapped and released with retardation in the main flow. Hauns et al. (2001) suggest that retardation and high dispersion provide evidence of an irregular conduit, including either numerous dispersive features or large-scale ones (e.g., chambers in our case). Their experiments have shown that singularities slow down the flow, increase the turbulence and produce eddies. The recirculation of the low-speed flow in the main flow will strongly influence the shape of the resulting breakthrough curve. Widiatmojo et al. (2015) also pointed out that D varied over the years, probably related to the closure of some mine branches (reduction in the mine size) and associated flow rate drops.

Speleological literature about cave air tracing is poor albeit several attempts have been reported, e.g. with injected CO_2 (Cella et al., 2015a, b; Gatti et al., 2015), SF_6, and CCl_2F_2 (De Freitas et al., 1982) as well as using natural tracers (Przylibski & Piasecki, 1998; Pflitsch & Piasecki, 2003) or artificially induced airflow (Lucas et al., 2013). Most studies aimed at obtaining information on air inlets/outlets or airflow rates but none of these attempted to derive geometric information about the conduit network nor tracer dispersion along natural conduits. It should be noted that certain tracers employed are currently classified as environmentally hazardous, i.e., SF_6 used in Thirnonsl & Kissel (1974), De Freitas et al. (1982), and Widiatmojo et al. (2015) or dangerous due to their flammability, e.g. C_2H_2 used in Standish (1988).

In this paper, we demonstrate that it is possible to gain reliable air flow rates and geometric information using CO_2 as an air tracer. As for hydro(geo)logical studies (Palmer et al., 1999; Hauns et al., 2001; Field, 2002), flow rates and geometrical parameters of the conduits can be derived from the information yielded by the tracer BTC. Moreover, we demonstrate that in the quite regular geometry of a mine, it is possible to assess the dispersion coefficient D using Chatwin's method (Chatwin, 1971), commonly used in hydrogeology. Finally, we suggest that the tailing observed with CO_2 in caves with complex geometry could be caused by the same singularities that would cause aerosol deposition.

METHODS

Site descriptions

Four CO_2-tracing tests were carried out in one naturally ventilated mine (artificial conduit, Baulmes Mine) and two ventilated caves (natural conduits, Milandre and Longeaigue caves). These conduits are subject to a chimney effect (Badino, 1995; Lismonde, 2002; Luetscher & Jeannin, 2004) and three of the four tests were carried out during an upward ventilation regime (with $T_{system} > T_{ext}$), while one was performed during a downward ($T_{system} < T_{ext}$) ventilation regime.

The cross-sectional areas were surveyed with several polar points (distance and inclination) measured along the conduit's perimeter using a modified Leica DistoX310 telemeter that provides tilt, azimuth and

distance (±0.05 m). In Milandre and Longeaigue, the cross-sections were surveyed every 10 m along the conduits of interest. In Baulmes the sections were surveyed every 10 m for the first 200 m, and every 20 m until 360 m. For each section, between 16 and 25 data points were surveyed. The sections were drawn within CAD software to determine the cross-sectional area with an estimated uncertainty of ±0.02 m² (Fig. 1).
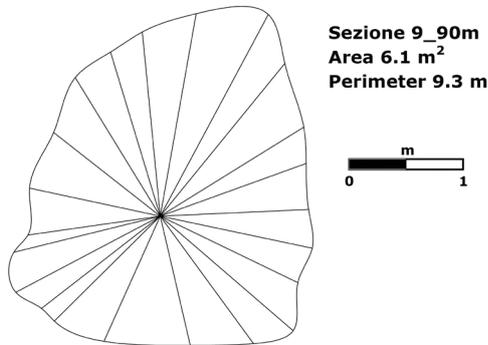

Sezione 9_90m
Area 6.1 m²
Perimeter 9.3 m

Fig. 1. Example of a vertical cross-section surveyed in Baulmes Mine (Section_9 at 90 m from the tunnel entrance).

Baulmes Mine

The Baulmes Mine (46°47'33" N 6°31'35" E, 655 m a.s.l.) was exploited during the first half of the 20th century for the production of lime and cement. The lower mine comprises 7 subhorizontal levels with a cumulated length of about 10.7 km (Fig. 2) (Deriaz et al., 2007). The difference in elevation between the lower and upper entrances reaches 90 m, ensuring a strong chimney effect. Tunnel #10 gives access to the lowest mine level with a 360 m-long sub-horizontal conduit reaching the main network of the mine. The geometry is typical of a mining tunnel: flat ground (except for some local collapses), vertical walls and a barrel-vaulted ceiling. Water flows in an occasionally open culvert from the innermost parts of the mine. No air inlets or outlets are observed along Tunnel #10, except for the main entrance. Three CO_2 data loggers were deployed at different stations (Fig. 2): for the test during the upward regime at 128 m (St_B3), 280 m (St_B4) and 360 m (St_B5) from the lower entrance; at 232 m (St_B3), at 270 m (St_B2) and 360 m (St_B1) for the test during the downward regime.
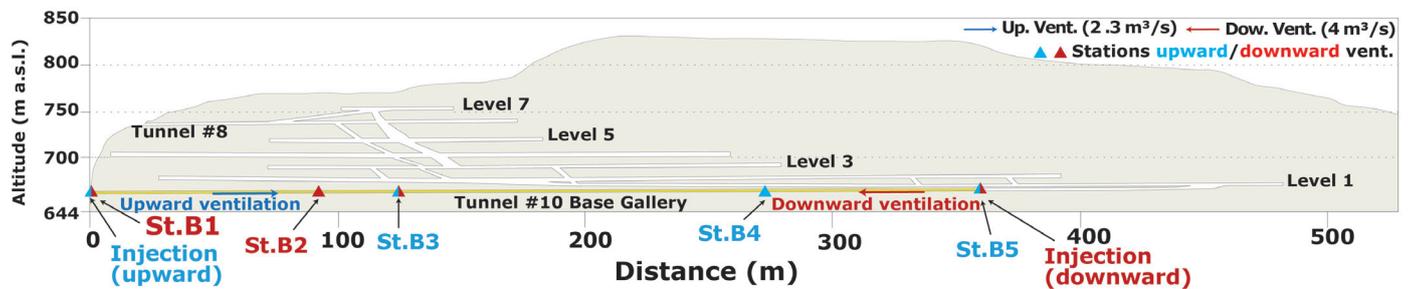

Fig. 2. Baulmes Mine ("mine inférieur"; Deriaz et al., 2007, modified). Blue shows the test stations during upward ventilation, red refers to the tests during downward ventilation.

Milandre Cave

The 10.5 km long Milandre Cave (47°29'6" N 7°0'58" E, 402 m a.s.l.), is located in Northern Switzerland on a limestone plateau at an elevation of about 500 m a.s.l. The main underground river passages cumulate 4.6 km between the upper to the lower entrances (135 m difference in elevation) (Jeannin et al., 2010). The cave complies with the chimney effect, ensuring permanent ventilation (downward or upward, according to the external temperature, Garagnon et al., 2022). The CO_2-gauging test was carried out in a 90 m long transect in the lower part of the cave (Fig. 3). Two measurement stations were deployed at, respectively, 20 (Mil_20) and 90 m (Mil_90 m) from the CO_2 release point.
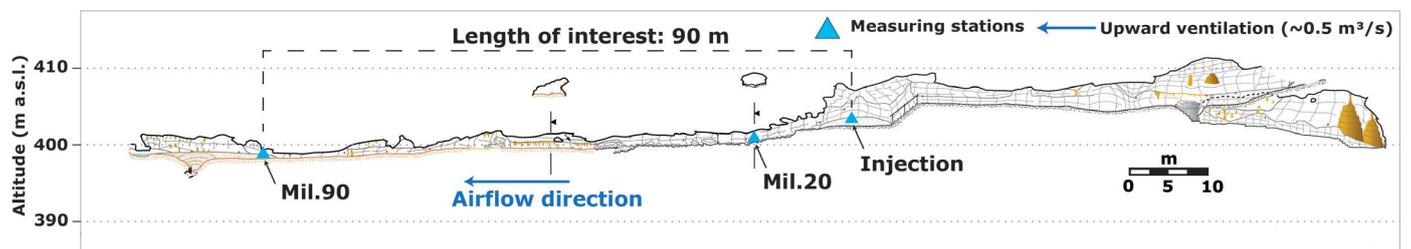

Fig. 3. An excerpt of the Milandre survey, showing the transect concerned by the CO_2 gauging test.

Longeaigue Cave

Longeaigue Cave lies in Val-de-Travers (Upper entrance: 46°52'22" N 6°31'09" E, 917 m a.s.l.; Lower entrance: 46°52'18" N 6°31'09" E, 820 m a.s.l.) and develops for 1.3 km. It is mainly dry and is crossed by an intense airflow due to the chimney effect developing between the two entrances. The elevation difference is 90 m with a distance of ~300 m between the two entrances. The CO_2 test was carried out along the main passage, releasing the gas close to the lower entrance and monitoring the gas breakthrough at 3 stations: Lo_239 (239 m from the injection point), Lo_278 (278 m from the injection point) and Lo_294 (294 m from the injection point). The cave is quite large until ~237 m, with extensive phreatic subhorizontal galleries showing some vadose reshaping (shafts) morphologies, and becomes narrower in the upper part where the cave has squeezing conduits. Between the stations Lo_294 and Lo_278 a secondary cave passage is present (red arrow in Fig. 4) which can cause airflow drops in this cave section.
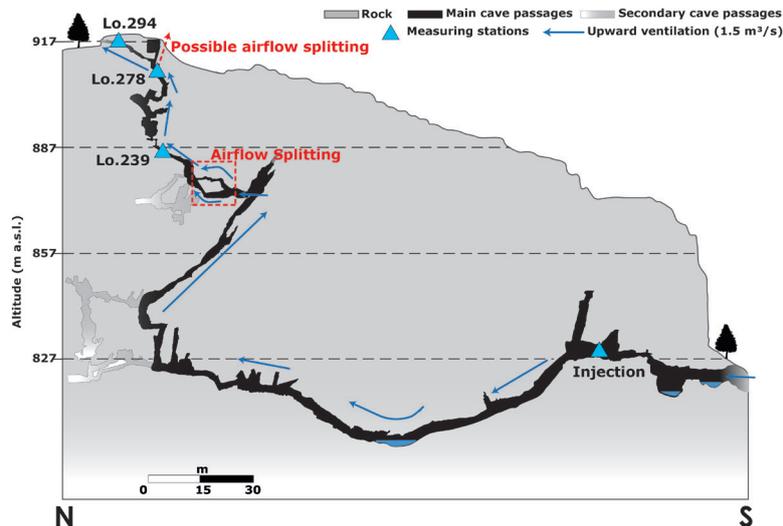
Fig. 4. An excerpt of the Longeaigue Cave survey, showing the transect concerned by the CO_2 gauging test. Modified after Jeannin (2018).

Comparison between the three sites

Twenty-eight cross-sections were surveyed in Baulmes, 10 in Milandre, and 30 in Longeaigue (Fig. 5). For all but the first 50 meters, the Baulmes tunnel shape is quite homogeneous (Fig. 5) showing a low standard deviation. In the first 128 m of the tunnel, the cross-section average is 6.4 ± 1.8 m² (n = 13) and from the entrance to the second station at 280 m it is 6.3 ± 1.3 m² (n = 29). Along the entire 360 m long tunnel the average cross-section was 6.6 ± 1.4 m² (n = 37). In Milandre Cave, the cross-section average of the first 20 m (Mil_20) is 10.8 ± 6.6 m² (n = 3), while the whole conduit of 90 m (Mil_90) has a mean cross-section of 6.3 ± 4.9 m² (n = 10). In Longeaigue Cave, the mean surveyed cross-section

from the injection station to the first station (Lo_239) of 7.4 m² ± 4.2 (n = 25), to the second station (Lo_278) of 7.0 ± 4.3 m² (n = 27) and to the last station (Lo_294) of 6.7 ± 4.3 m² (n = 29). The standard deviation of averaged cross-sections makes it possible to state that Longeaigue and Milandre natural conduits have a less uniform distribution of the cross-sections over a smaller distance than Baulme's anthropic tunnel and that cross-section variations in Baulmes are less pronounced than in Longeaigue and Milandre (Fig. 5). Moreover, the changes in cross-section dimensions between two measurement points along Longeaigue are sharper than in Milandre and appear distributed all along the conduit. Only the last 40 m of Longeaigue (Fig. 5) show a more uniform distribution of small cross-sections.
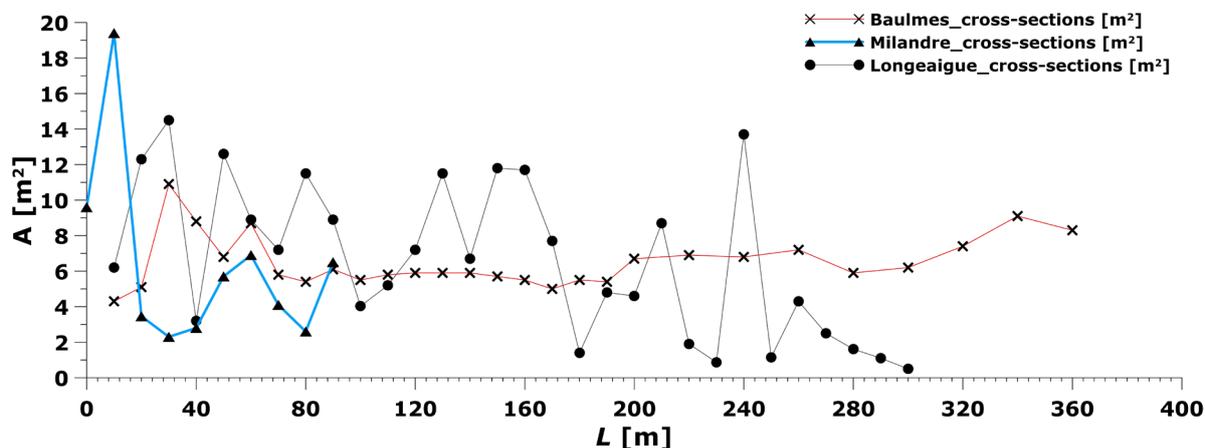

Fig. 5. Cross-section surface areas measured along the investigated conduits in Baulmes Mine, Milandre and Longeaigue caves.

Instrumentation

A tank of 1.5 kg CO_2 (2 L, $5.7 \cdot 10^3$ kPa) was used to release the tracer. The tank was provided with a faucet valve. Hence, to ensure that $t_{release} < t_{transit}$ it was opened for 1 to 2 minutes (depending on the travel distance). The released CO_2 mass (± 0.05 kg) was obtained by weighing the tank before and after each test. CO_2 was monitored at 1 min in Baulmes and 20 sec time intervals in Milandre and Longeaigue, using SCD-41 CO_2 sensors (Adafruit; device accuracy ± 50 ppmv +5% of reading) implemented on a 3.3 V microcontroller based on I2C protocol, functioning as

a data logger. The error on measured concentrations is generally between 10% and 15%. The background CO_2 concentration was measured between thirty minutes and an hour before the tracer release, showing no significant variation (<50 ppmv). Therefore, it was assumed that the background CO_2 concentration remained constant during the tracer travel time (ranging from 10 minutes to 1.5 hours, depending on the site) and was subsequently subtracted from the raw data. The impact of anthropogenic exhaled CO_2 can be neglected (only two people, who left the site immediately after the injection). The maximum

concentration at the injection point for each site was estimated through mass conservation. It ranged between $2\cdot10^3$ (at Baulmes Mine) and $20\cdot10^3$ mg/m³ (at Milandre Cave with the lowest flow rate).

A hand-held hotwire anemometer (Testo 425; device accuracy ±0.03 m/s +5% of reading) was used to measure the flow in the conduits by integration of 6 measurements averaged over 30 s at each cross-section. Results are compared with airflow inferred from the CO_2 gauging, assumed constant during the tests.

Theoretical approaches

Airflow gauging

Tracing experiments are based on the dispersion and mass conservation of an artificial tracer in a fluid flow. The airflow rate can be derived by Eq. 1 below:

$$Q = \frac{m}{\int c(t)\,dt} \approx \frac{m}{\sum_{i=0}^{k}\left(c_{i_{CO_2}}\,\Delta t\right)}$$

where Q is the airflow rate [m³/s], m is the known mass of the injected tracer [g], c is the measured concentration [ppmv] at time t [s].

It is worth noting that Eq. 1 provides an accurate estimation of the flow rate Q if mass conservation is satisfied, i.e., if there is no leak between the injection point and the sensor. If this condition is not well-constrained in the field, Eq. 1 might yield wrong results.

The mean air speed U and the mean cross-sectional area A can be determined by a quantitative analysis of the BTCs. The mean velocity of the tracer (U_p) is obtained by dividing the travel distance by the time to the BTC peak (max value) (Eq. 2):

$$U_p = \frac{L}{t_{peak}}$$

The mean residence time $\bar{t}$ [s] (Eq. 3), namely, the time required for the mass of the tracer to traverse the entire length L [m], for a short-pulse release is given by Gaspar (1987) and modified by Field (2002):

$$\bar{t} = \frac{\int_0^\infty t\,C(t)\,Q(t)\,dt}{\int_0^\infty C(t)\,Q(t)\,dt}$$

For a constant flow rate Q, the volume V [m³] of air crossing the entire length L during the test is given by Eq. 4:

$$V = Q\,\bar{t}$$

and the mean cross-section A [m²] along the length L is given by Eq. 5:

$$A = \frac{V}{L}$$

Numerical evaluation of the BTCs

At a distance from the injection point much larger than the pipe diameter, the 1-D dispersion-advection equation (Eq. 6) (Taylor, 1954) reads:

$$\frac{\partial C}{\partial t} + U\frac{\partial C}{\partial x} = D\left(\frac{\partial^2 C}{\partial x^2}\right)$$

where C is the solute concentration averaged over the cross-section, U is the mean air velocity, t is the time and x represents the distance from the injection point. In the following, we consider the case of a single

airway of constant cross-section A with a probe at a length L from the injection point where a mass m of tracer has been injected at time $t = 0$. A long-time asymptotic solution of Eq. 6 at the probe location is given by Taylor (1954) and Chatwin (1971) in Eq. 7:

$$C(t) = \frac{m}{A\,\sqrt{4\pi Dt}}\exp[-\frac{(L-Ut)^2}{4Dt}]$$

A necessary condition of validity of Eq. 7 is $t \gg D/U^2$. Eq. 7 is adopted independently for water (Field, 1999, 2002; Hauns et al., 2001; Massei et al., 2006) and air (Widodo et al., 2008; Sasaki et al., 2009; Widiatmojo et al., 2015;). Eq. 7 depends only on the flow velocity and geometrical characteristics of the conduit. The concentration variations over the cross-section being much smaller than in the longitudinal direction, we assume that the local concentration provided by the probe is a good approximation of the cross-section averaged concentration C included in Eq. 6 and Eq. 7.

The Chatwin geometrical method to assess D

The geometrical method proposed by Chatwin (1971) is often adopted to assess the hydro(geo)logical dispersion coefficient D (Field, 1999, 2002; Hauns et al., 2001; Massei et al., 2006). It consists in rewriting Eq. 7 as shown in Eq. 8 below:

$$\sqrt{t_i\,\ln\left(\frac{C_{peak}\,\sqrt{t_{peak}}}{C_i\,\sqrt{t_i}}\right)} = \left|\frac{L}{2\sqrt{D}} - \frac{U}{2\sqrt{D}}t_i\right|$$

where C_i is the concentration at the instant t_i, while C_{peak} is the peak concentration at the corresponding instant t_{peak}. If Eq. 7 is valid, plotting the left side of Eq. 8 against time yields two straight lines of equation (Eq. 9):

$$y = \frac{L}{2\sqrt{D}} - \frac{U}{2\sqrt{D}}t$$

which provides the dispersion coefficient D and the fluid mean velocity U by linear regression. In an ideal case $U = U_p$.

RESULTS

CO_2 breakthrough curves

Instances of BTCs measured at the last station of each site are shown in Figure 6. The time t and the concentration C have been normalized by the coordinates of the concentration peak t_{peak} and C_{peak}, respectively. For the Baulmes test, points are quite symmetrically distributed around $t^* \equiv t/t_{peak} = 1$. Instead, BTCs from caves show a more asymmetrical shape, with a significant part of the distribution included in the time range from $t^* = 1.5$ to 2.5. Because the external temperature did not vary significantly during the tests, the internal airflow is assumed constant and the extended tails likely result from the more irregular geometry of caves compared to Baulmes' artificial conduit (see Fig. 5). In the case of Milandre Cave, the background concentration was not fully recovered because the CO_2 was released in a chamber (Fig. 3) favouring tailing due to air recirculation and diffusion.

Airflow rate and conduit geometry

To infer the airflow, tracer mass conservation is assumed for all the tests to solve Eq. 1. The results between gauged and directly measured airflow are

compared in Table 1. The relative deviation between CO_2 gauged airflow and the direct measurements (Table 1) consistently stays below 5% in Baulmes.

However, this difference expands to around 30% in Milandre and can rise to as much as 47% at the last Longeaigue probe, between Lo_294 and Lo_278.
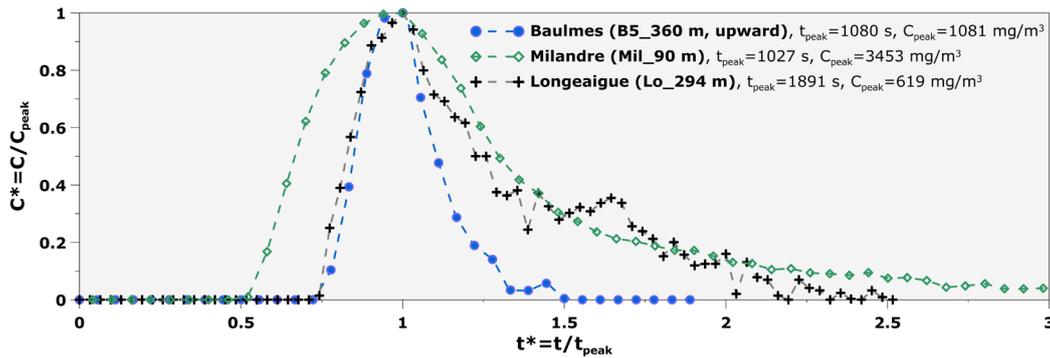

Fig. 6. Instances of CO_2 BTCs for the three investigated sites (normalized concentrations and times). All points are shown at a logging rate of 60 seconds.

Table 1. Gauged air flowrate Q_{CO_2} and manually measured air flowrate Q_m in Baulmes, Milandre and Longeaigue.

Site	Injected mass (kg)	Station	Q_{CO_2} [m³/s]	Q_m [m³/s]	$(Q_m-Q_{CO_2})/Q_{CO_2}$
Baulmes (upward) 2/15/23 9:30	0.78	St_B3	2.3	2.3	0
		St_B4	2.1	-	-
		St_B5	2.3	-	-
Baulmes (downward) 5/2/23 17:08	1.00	St_B3	3.8	4	0.05
		St_B2	3.7	-	-
		St_B1	3.6	-	-
Milandre 2/8/22 12:20	1.00	Mil_20	0.39	0.52	0.33
		Mil_90	0.35	-	-
Longeaigue 12/13/22 15:14	1.00	Lo_239	1.5	1.76	0.17
		Lo_278	1.5	-	-
		Lo_294	1.5	0.79	-0.47

From the analyses of the BTCs, it was possible to infer the average cross-sections (A_{CO_2}) at the gauging stations (Eq. 5). The twenty-eight surveyed cross-sections (Fig. 5) were averaged (A_{avg}) for each station, enabling the comparison with CO_2-gauged cross-sections (A_{CO_2}). The results are presented in Table 2 for Baulmes Mine, Milandre and Longeaigue caves.

The differences between A_{avg} and A_{CO_2} at Baulmes Mine were within 1.5% and 3.2%, showing a good agreement between the inferred and surveyed cross-sections for both ventilation regimes. In Milandre Cave the disagreement between the two methods was higher. The average cross-section evaluated by the CO_2 gauging along the 90-m-long conduit in Milandre

(Mil_90) is smaller than the surveyed one by 20%. However, it is within the variability of this cave transect (st.dev. ±4.9 m²). Lastly, cross-sections gauged in Longeaigue show differences of up to 74% (Lo_294) from those obtained by the *in situ* survey (Table 2). Although even in Longeaigue the relative difference between the two methods is within the variability of the surveyed cross-sections, the agreement between A_{avg} and A_{CO_2} is noticeably worse compared to that of Milandre. This higher difference can be attributed to the presence of more complex cave morphologies (Fig. 5 and Table 2) generating the long tail evident in the raw data from Longeaigue (Fig. 6) which can influence the estimation of conduit volumes (Eq. 4) and cross-sections (Eq. 5).

Table 2. Comparison between the surveyed cross-sections together with results inferred from the CO_2 gauging at different sites. A_{avg}: average cross-sections from the injection point to the station; A_{CO_2}: average cross-section inferred from CO_2 tracer velocity.

Site	Station	A_{avg} [m²] ± 1σ	A_{CO_2} [m²]	$(A_{CO_2}-A_{avg})/A_{avg}$
Baulmes (upward)	St_B3	6.4±1.8 (n=13)	6.5	0.02
	St_B4	6.3±1.4 (n=29)	6.5	0.03
	St_B5	6.6±1.4 (n=37)	6.7	0.02
Baulmes (downward)	St_B3	6.6±1.2 (n=25)	6.4	-0.03
	St_B2	6.5±1.1 (n=29)	6.5	0
	St_B1	6.6±1.4 (n=37)	6.5	-0.02
Milandre	Mil_20	10.8±6.6 (n=3)	10.5	-0.03
	Mil_90	6.4±4.9 (n=10)	5	-0.2
Longeaigue	Lo_239	7.5±4.1 (n=25)	11.2	0.49
	Lo_278	7.2±4.1 (n=27)	11.3	0.6
	Lo_294	6.8±4.2 (n=29)	11.8	0.74

Data analysis: dispersion coefficient D and curve simulations

U and D were fitted using Eq. 9 after plotting the left side of Eq. 8 as a function of time (see the insets in Fig. 7). In Milandre and Longeaigue caves, the model cannot reproduce the last part of the data sets where the tailing is accentuated. Therefore, this part of the curves (blue dots in the insets of Fig. 7) was not considered in the fit. Conversely, the complete data sets of Baulmes were taken into account. In all cases, a high correlation between the selected data and the fitting lines was obtained ($R^2 \geq 0.97$, see Fig. 7). Since Eq. 2 and Eq. 9, both give average airspeeds (U_p and U respectively), it was verified that the ratio $(U-U_p)/U_p$ never exceeds $\pm 2\%$, so that $U_p = U$ can be assumed. As expected from the fit of U and D, the simulated BTCs (Fig. 7) match always well with the empirical data from Baulmes, whereas the simulation does not reproduce the last part of the BTCs in Longeaigue and Milandre, where the concentration decreases more slowly compared to an exponential model (Eq. 7).

Discussing the dispersion coefficients obtained in Milandre and Longeaigue is not meaningful, since they are estimated using Eq. 7, which fails to describe the BTCs. The dispersion coefficient D in Baulmes is of the order of 1 m²/s (see Table 3). It is slightly larger for downward flow, which is consistent with the higher air velocity during this test. Surprisingly, D slightly varies with the distance of the sensor from the injection point, for both tests (downward and upward flows).

Table 3. Length of the conduit transects L, aeraulic diameters d ($d = 4 \cdot A$ / perimeter, derived from surveyed cross-sections), peak velocity U_p, dispersion coefficients D inferred from field data, dispersion coefficients D_T predicted by the Taylor's theory (Eq. 5), the ratio D/D_T. The uncertainty range on D_T results from the uncertainty on the Darcy friction coefficient.

| Site	Station	L [m]	d [m]	U_p [m/s]	D [m²/s]	D_T [m²/s]	D / D_T
Baulmes (upward)	St_B3	128	2.6	0.36	1.39	[0.40 – 0.51]	[2.7 – 3.5]
	St_B4	300	2.6	0.36	0.83	[0.40 – 0.51]	[1.6 – 2.1]
	St_B5	360	2.6	0.36	0.87	[0.40 – 0.51]	[1.7 – 2.2]
Baulmes (downward)	St_B3	232	2.6	0.64	1.98	[0.64 – 0.82]	[2.4 – 3.1]
	St_B2	270	2.6	0.56	1.71	[0.64 – 0.82]	[2.1 – 2.7]
	St_B1	357	2.6	0.56	1.3	[0.64 – 0.82]	[1.6 – 2.0]
Milandre	Mil_20	20	2.6	0.13	0.64	-	-
	Mil_90	90	1.6	0.12	0.57	-	-
Longeaigue	Lo_239	239	2.6	0.18	1.41	-	-
	Lo_278	278	2.6	0.17	0.75	-	-
	Lo_294	294	2.4	0.16	0.7	-	-
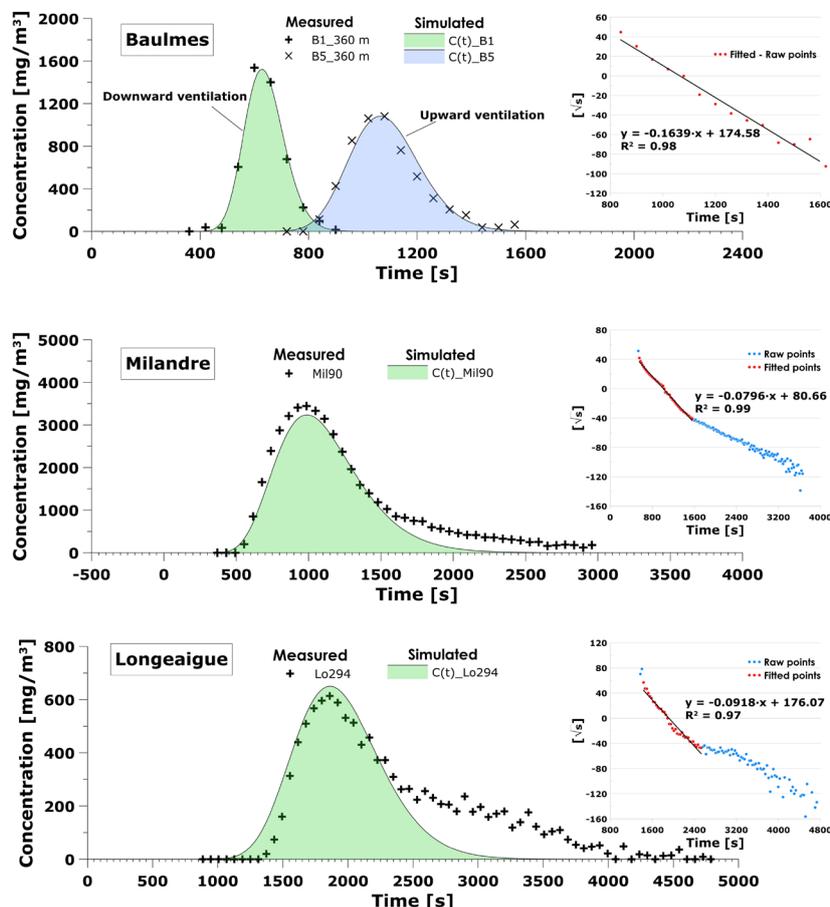
Fig. 7. Measured CO$_2$ concentrations (crosses) and simulated BTCs (Eq. 7) at each site. Results obtained at intermediary stations are shown in Table 3. Insets: left side of Eq.8 (dots) and fit using Eq. 9 (solid line). In orange are the points selected for the fit.

DISCUSSION

Four CO_2 tests were carried out in one mine (artificial conduit) and two ventilated caves (natural conduits), to investigate the reliability of the method for gauging airflow (Fig. 6), assessing average cross-sections (Table 2) and inferring the dispersion value along ventilated karst conduits (Table 3 and Fig. 7).

The gauging tests were consistent with most of the independent measurements performed manually with an anemometer. The difference between the gauged airflow and the manual measurements generally ranges between 0 and 33%. An exception is station Lo_294 in Longeaigue, where the difference reached 47% when the airflow was measured at 0.78 m³/s against 1.5 m³/s inferred from CO_2-gauging.

The first possible explanation could be related to the 3-hour difference between the manual measurement and the injection time, which was much higher than for the other sites. However, the temperature difference between the cave and the outside temperature, which drives the airflow inside the cave by a chimney effect, was larger at the moment of the manual measurement than during the CO_2 gauging. Therefore, the flow rate measured manually should have been higher than the flow rate obtained from CO_2 gauging, in contrast to what has been observed. Alternatively, the manually measured airflow may have been impacted by the presence of the operator in the 0.5 m² narrow conduit. Another possible reason for this deviation can be related to the assumption of mass conservation (Eq. 1) which could possibly not be correct if the system under investigation is not well-constrained and known. If in Milandre and Baulmes the absence of air divergences is warranted, it is not possible to say the same for Longeaigue. As shown in Table 1, the information of a possible leak (53% of the mass) is given by direct measurements, otherwise not visible only through the gauging test. As observed, the divergence located between Lo_239 and Lo_294 (dashed red arrow in Fig. 4) could provoke sometimes a secondary airflow reducing the airflow at the upper entrance. More investigation will be necessary to clarify this point. To determine the airflow, the basic assumption of air mass conservation has to be verified, otherwise the gauged airflow may be unreliable. However, the presence of an air leak could be checked with the gauging technique by installing a logger along the possible leakage conduit, to confirm or not the passage of injected CO_2. Therefore, a good knowledge of the studied site is fundamental to make sure that mass conservation is assured.

Air velocity can be referred to as a local velocity or as an average velocity along a conduit. The first can be inferred by spot measurements with e.g. anemometers, while the second requires gauging tests and can be represented by BTC peak velocity (U_p in Table 3). In caves, punctual air velocity is usually measured in cross-sections where the air draft is sufficiently strong to be measured, i.e. in narrow passages. Therefore, spot measurements are unlikely to yield an average air velocity over the entire length of the cave. Moreover, high uncertainties are expected at low air velocities,

such as when the cross-sections are large or in the presence of a small driving force (e.g., in caves with a small vertical distance between entrances or tiny ΔT between external and internal atmosphere) (Faimon & Lang, 2013; Gabrovšek, 2023). In particular, at low speeds, measurements can be significantly affected by instrumental accuracy (e.g., accuracy of ±0.03 m/s compared to measurements of 0.15 m/s) and would require high-resolution monitoring with digital devices (Pastore et al., *in review*). Therefore, the CO_2 gauging test is a reliable method for assessing airflow rate under low-velocity conditions.

The regularity of the gallery in Baulmes (Fig. 5) ensures a consistent result between the CO_2-inferred cross-sectional areas and the surveyed mine sections (Table 2), with an instrumental accuracy on cross-section (A_{CO_2}) assessment between ±5% and ±7%. In contrast, in Milandre and Longeaigue caves, the difference between A_{avg} and A_{CO_2} reaches 20% and 74%, respectively. Although the surface areas inferred by the CO_2 gauging tests are included in the natural variability of the conduit geometries, the mismatch can be due to 1) the estimation of the mean tracer residence time $\bar{t}$ (Eq. 3) or 2) the low spatial resolution (10 m) of the *in situ* survey. In Longeaigue, sudden and systematic changes in diameter (Figs. 4, 5), bends and air splitting (dashed rectangle in Fig. 4) are present. Narrow passages whose cross-sections are between 0.5 and 1.1 m² were surveyed throughout the cave (Fig. 5), and the largest cross-sections are found between these passages, forcing the air to continuously constrict and expand, causing tailing and lagging (high $\bar{t}$). Larger cross sections will slow down the transport by decreasing the air velocity, increasing the residence time $\bar{t}$. A higher $\bar{t}$ will be reflected in an overestimation of the average conduit volume (Eq. 4) and thus an overestimation of the average conduit cross-section (Eq. 5). Consequently, dead flow zones and air recirculation causing the tailing likely lead to a better representation of larger cross-sections. The second reason for the discrepancy may be that, in a cave, changes in the cross-sectional area occur at a resolution of less than a few meters and the average surface areas present a large standard deviation. Therefore, the 10-m resolution surveyed at Milandre and Longeiague may not be fully representative. For instance, the 90 m-long Milandre conduit is more variable than the Baulmes tunnel over 360 m, showing standard deviations of ±4.9 m² and ±1.8 m², respectively. In Longeaigue Cave, the variability of the cross-section is even more marked than in Milandre. The lower part of Longeaigue Cave (from the injection point to the station Lo_239) presents morphologies characterized by shafts, rockfalls, and narrow passages alternating with chambers and galleries. In contrast, the upper part of the cave is mainly characterized by rounded narrow passages (from Lo_239 to Lo_294). The number of surveyed cross-sections necessary for a representative average in a cave may be difficult to assess.

Simplifying the characterization of flow and dispersion in complex conduits is not straightforward. Gauging tests proved to yield a first piece of information

about average cross-sections and average velocity along the conduit, both necessary for appropriate modelling. Using CO_2 as a tracer across different ventilated systems brings values for average cross-sections and conduit volumes, which can be compared to cave mapping. Cave cross-section errors brought about by the CO_2 tests along complex ventilated cave conduits can be reduced by carrying out CO_2 tests on shorter conduit transects, aiming to minimize the tailing effect. These geometrical parameters can allow the comparison of such values between different caves and could enable the definition of new morphometric indices such as the ratio of a system's volume to its average cross-sectional area and length (Piccini, 2011). These analyses are of particular interest in geoplanetology when comparing terrestrial lava tube morphologies and similar features observed on the Moon and Mars (Sauro et al., 2020; Bell et al., 2022). Sauro et al. (2013) applied several methods to infer the average cross-section of terrestrial lava tubes, either through 3-D surveys or by extrapolating the mean height and width from speleological surveys. In the presence of airflow, CO_2-gauged geometries could prove useful in advancing this new field of research.

Comparison with Taylor's theory

For Baulmes tests, it is interesting to compare the dispersion coefficients estimated from the field data with the prediction of Taylor's theory that implicitly assumes the validity of Eq. 7, comparisons with results from Milandre or Longeaigue would not make sense. The Reynolds number $Re = 4 \cdot Q_{CO_2} / p \cdot v$ (with p the conduit perimeter derived from surveyed cross-sections, and $v = 1.43 \cdot 10^{-5}$ m²/s the air kinematic viscosity) was of the order of 10^5 during Baulmes tests, clearly indicating turbulent airflow. Taylor's (1954) prediction for the turbulent regime reads like in Eq. 10:

$$D_T = 5.05 \; d \; U^*$$

where the friction velocity U^* is related to the mean velocity U_p by the relation in Eq. 11 below (Widiatmojo et al., 2015):

$$U^* = U_p \times \sqrt{\frac{f}{8}}$$

where f is the Darcy friction factor, which depends on Re and the relative roughness $\varepsilon_r = \varepsilon / d$ (with $d = 4 \cdot A / p$ the hydraulic diameter of the conduit). The wall's absolute roughness ε is not accurately known, but we estimate that it should be in the range of 10 to 30 cm. The Moody chart (Moody, 1944) yields the corresponding friction factors f ranging from 0.06 and 0.1. Entering these values in Eq. 11 and Eq. 10 provides the uncertainty range of D_T displayed in Table 3.

Our results reveal that the dispersion coefficient D estimated from Baulmes BTCs is systematically 1.6 to 3.5 times higher than the prediction from Taylor's theory (see Fig. 8 and Table 3). Instrumental uncertainties, which represent ±15% of D, cannot explain these descrepancies. Moreover, Taylor's theory is known to be accurate for $Re \gtrsim 2 \cdot 10^4$, a condition that is verified since we obtained $Re \sim 10^5$ during the tests. A first possible explanation for the discrepancy

between the theoretical D_T and experimental D could be that Baulmes Tunnel #10 is not strictly circular (see Fig. 1), as assumed in Taylor's theory. Moreover, the section of Baulmes Mine, although much more regular than caves, significantly varies throughout the conduit (see Fig. 5). Assessing the consequences of these geometrical "defects" is not possible with the available data. Our results are nonetheless consistent with those obtained by Widiatmojo et al. (2015) (Fig. 8), which also identified enhanced dispersion along mine conduits compared to Taylor's predictions. These authors suggested that the high dispersion coefficients measured in the Kushiro Mine could be related to the presence of cavities along the mine tunnels, which trap the tracer and reintroduce it into the main flow with a delay. The absence of such cavities along the Baulmes Tunnel #10 is consistent with a lower dispersion coefficient, closer to Taylor's theory.

Taylor's theory is relevant neither in caves nor in mines, even though the conduit geometry is more regular in the latter case. However, a 1-D simulation based on Eq. 6 is still possible in mines, using empirical dispersion coefficients deduced from field data (see Baulmes results in Fig. 7). Note that in this site, the inferred D at the last station (B1 or B5 according to the flow direction) is intended to represent the average D value for the entire conduit length (L = 360 m). However, because D decreases systematically with increasing L, if a D value corresponding to a shorter length than L (e.g., to B3 or B2) is assigned for the simulation, this will result in an overestimation of the peak concentration.

BTC analysis displayed an accentuated tailing along the investigated natural conduits due to the presence of dispersive singularities which possibly enable aerosol deposition. For example, the long tailing observed in Milandre and Longeaigue caves is probably due to cross-section variations. Additionally, the 1-D advection-dispersion model was found to be unable to fit BTC tailing. Along natural caves, airways encounter bends, bottlenecks, collapses, variable wall roughness, speleothems, and other structural factors which are absent in the artificial conduit of Baulmes Mine. This is a key point that will likely impact the air movement and consequently the airborne aerosol distribution and settlement. Therefore, a more complex model is required. Addesso et al. (2022) showed that, in caves, changes in fluid dynamics occur where these singularities are present, resulting in the deposition of airborne particles. Therefore, the tailing observed in CO_2 tests could suggest that, in the case of airborne matter, an increased tailing corresponds to greater sedimentation along the investigated conduit. Hauns et al. (2001) highlighted that retardation could result from the presence of dispersive structures if those have a storage time at the same order of magnitude as the duration of the tracer BTC. Therefore, tailing duration allows an estimate of how long matter can be trapped in low-velocity structures. Stokes' law reads that areas of slow flow (dead flow zones) are favourable to the deposition of aerosols transported in a fluid (e.g. air). Dead flow zones cause the deposition of suspended

matter and the quantity of deposited matter is somehow proportional to the tailing duration. Hence, along natural karst conduits, the variable geometry and presence of obstacles lead to dead flow zones. Those dead flow zones (e.g., chambers) retard the transport producing tailing and modify the dispersion with distance. For instance, in the case of Longeaigue, the tailing suggests that larger chambers with a low air velocity are more prone to deposition than narrower ventilated conduits.
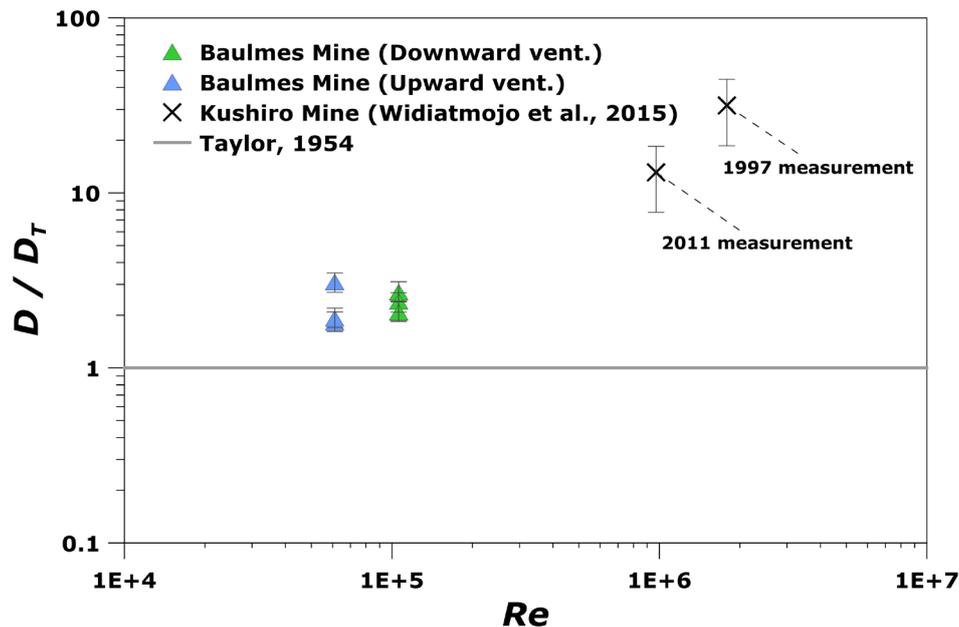

Fig. 8. Comparison between the dispersion coefficient obtained from BTCs and Taylor's theory for the Baulmes Mine (this work) and Kushiro Mine (Widiatmojo et al., 2015). The vertical error bars correspond to the uncertainty on Darcy's friction factor required to estimate D_T.

CONCLUSIONS

In the karst vadose zone, cave ventilation is an efficient mode of transport for heat and aerosols and drives the spatial distribution of airborne particles in a cave system. Modelling this airborne transport requires geometrical and physical parameters of the conduit system, including the cross-section areas, the airflow and average air speed, as well as the dispersion coefficient which describes the spread of a solute. The four experiments carried out in natural and artificial conduits, by using CO_2 as a tracer, showed to be a suitable technique to infer the airflow and average conduit cross-sections. The value of dispersion has also been inferred by applying Chatwin's method. BTC analysis displayed an accentuated tailing along the investigated natural conduits due to the presence of dispersive singularities which possibly enable aerosol deposition. The long tailing observed in Milandre and Longeaigue caves is probably due to cross-section variations, therefore chambers are likely prone to deposition. In contrast with Longeaigue and Milandre caves, the 1-D advection-dispersion model correctly reproduces the shape of the BTCs in the Baulmes Mine. However, Taylor's (1954) theory significantly underestimates the dispersion coefficient deduced from the BTCs. Numerical simulations of 3-D Navier-Stokes equations would be interesting to investigate solute dispersion in caves and mines, in particular, to assess the role of the conduit geometry. It was already attempted for water flow (Hauns et al., 2001). Similar works should be done for airflow.

This paper gives a first insight into air motion and matter dispersion along ventilated karst conduits, preparing for proper aerosol dispersion modelling.

ACKNOWLEDGEMENTS

Authorship statement: CP, ML, and PYJ designed and directed the study. EW developed the electronic devices used for the measurements. CP performed the measurements and analyzed the data. CP and FD carried out the simulations. CP wrote the paper with input from all authors.

REFERENCES

Addesso, R., Pingaro, S., Bisceglia, B., Baldantoni, D., 2022. Sustainable tourism and conservation of underground ecosystems through airflow and particle distribution modeling. Sustainability, 14, 7979. https://doi.org/10.3390/su14137979

Badino, G., 1995. Fisica del clima sotterraneo, Memorie dell'Istituto Italiano di Speleologia. Società Speleologica Italiana.

Bell, E., Schmerr, N., Young, K., Esmaeili, S., Garry, W.B., Jazayeri, S., Kruse, S., Richardson, J., Whelley, P., 2022. Field mapping and modeling of terrestrial lava tube magnetic anomalies as an analog for lunar lava tube exploration and prospecting. Journal of Geophysical Research, Planets, 127, e2021JE007140. https://doi.org/10.1029/2021JE007140

Cella, G.D., Gigante, D., Miragoli, M., 2015a. Test con traccianti aerei ai piani del tivano (Co). In: Nitto, L.D.,

Maurano, F., Parise, M. (Eds.), Atti XXII Congresso Nazionale di Speleolgia "Condividere i Dati." Memorie dell' Istituto Italiano di Speleologia, p. 463–468.

Cella, G.D., Gigante, D., Miragoli, M., 2015b. Tracciamento delle correnti aeree con Terpeni Naturali. In: Nitto, L.D., Maurano, F., Parise, M. (Eds.), Atti XXII Congresso Nazionale Di Speleolgia "Condividere i Dati." Memorie dell' Istituto Italiano di Speleologia, p. 478–485.

Chatwin, P.C., 1971. On the interpretation of some longitudinal dispersion experiments. Journal of Fluid Mechanics, 48, 689–702. https://doi.org/10.1017/S0022112071001800

Christoforou, C.S., Salmon, L.G., Cass, G.R., 1996. Fate of atmospheric particles within the Buddhist Cave Temples at Yungang, China. Environmental Science and Technology, 30, 3425–3434. https://doi.org/10.1021/es950875r

Christoforou, C.S., Salmon, L.G., Cass, G.R., 1994. Deposition of atmospheric particles within the Buddhist Cave Temples at Yungang, China. Atmospheric Environment, 28, 2081–2091. https://doi.org/10.1016/1352-2310(94)90475-8

De Freitas, C.R., Littlejohn, R.N., Clarkson, T.S., Kristament, S., 1982. Cave climate: assessment of airflow and ventilation. Journal of Climatology, 2, 383–397. https://doi.org/10.1002/joc.3370020408

Deriaz, P., Bourret, F., Jeannin, P., Lalou, J., Lambelet, J., Pauli, C., Spring, D., Thévoz, D., 2007. Inventaire spéléologique de la suisse, Tome V, Nord vaudois. Commission de Spéléologie de l'Académie Suisse des Sciences Naturelles, La Chaux de Fonds.

Dredge, J., Fairchild, I.J., Harrison, R.M., Fernandez-Cortes, A., Sanchez-Moral, S., Jurado, V., Gunn, J., Smith, A., Spötl, C., Mattey, D., Wynn, P.M., Grassineau, N., 2013. Cave aerosols: distribution and contribution to speleothem geochemistry. Quaternary Science Reviews, 63, 23–41. https://doi.org/10.1016/j.quascirev.2012.11.016

Faimon, J., Lang, M., 2013. Variances in airflows during different ventilation modes in a dynamic U-shaped cave. International Journal of Speleology, 42(2), 115–122. https://doi.org/10.5038/1827-806X.42.2.3

Faimon, J., Ličbinský, R., Lang, M., Überhuberová, J., Hebelka, J., 2019. Cave microclimatology: diurnal variations in aerosol particle concentrations. Theoretical and Applied Climatology, 137, 2841–2852. https://doi.org/10.1007/s00704-019-02776-1

Field, M., 2002. The QTRACER2 program for tracer-breakthrough curve analysis for tracer tests in karstic aquifers and other hydrologic systems. US Environmental Protection Agency, 600/R-02/001, 179 p.

Field, M.S., 1999. Quantitative analysis of tracer breakthrough curves from tracing tests in karst aquifers. Karst modeling. Special publication 5, 163–171.

Gabrovšek, F., 2023. How do caves breathe: The airflow patterns in karst underground. PLoS ONE, 18, e0283767. https://doi.org/10.1371/journal.pone.0283767

Garagnon, J., Luetscher, M., Weber, E., 2022. Ventilation regime in a karstic system (Milandre Cave, Switzerland). Proceedings of the 18th International Congress of Speleology, Savoie Mont Blanc, 3, 187–190.

Gaspar, E., 1987. Modern trends in tracer hydrology. CRC Press, Boca Raton, 145 p.

Gatti, F., Pozzo, M., Cella, G.D., 2015. Sistema Carsico Bueno Fonteno - Nueva Vida: Studio e tracciamenti dei flussi d'aria. In: Nitto, L.D., Francesco, M., Parise, M. (Eds.), Atti XXII Congresso Nazionale Di Speleolgia "Condividere i Dati." Memorie dell' Istituto Italiano di Speleologia, pp. 486–491.

Hart, J., Guymer, I., Jones, A., Stovin, V., 2013. Longitudinal dispersion coefficients within turbulent and transitional pipe flow. In: Rowiński, P. (Ed.), Experimental and computational solutions of hydraulic problems. GeoPlanet: Earth and Planetary Sciences. Springer, Berlin, p. 133–145. https://doi.org/10.1007/978-3-642-30209-1_8

Hauns, M., Jeannin, P.Y., Atteia, O., 2001. Dispersion, retardation and scale effect in tracer breakthrough curves in karst conduits. Journal of Hydrology, 241, 177–193. https://doi.org/10.1016/S0022-1694(00)00366-8

Hauns, M.C., 1999. Modeling tracer and particle transport under turbulent flow conditions in karst conduit structures. Unpublished PhD Thesis, Université de Neuchâtel, 78 p.

Higgins, J., Shuttleworth, S.E.H., 1958. A tracer gas technique for the measurement of airflow in headings. Colliery Engineering, 35, 483–487.

Jeannin, P.-Y., 2018. La Baume de Longeaigue. 30 ans de silence. Cavernes, 32–49.

Jeannin, P.Y., Weber, E., Wenger, R., Meury, P.X., 2010. High CO_2 concentrations and cave ventilation test in the Milandre Cave, Jura mountains, Switzerland. Proceedings of the 15th International Congress of Speleology, Kerville (TX), 2, 534–538.

Lismonde, B., 2002. Climatologie du monde souterrain. tome 2: Aérologie des systèmes karstiques. Comité Départemental de Spéléologie de l'Isère, 362 p.

Luetscher, M., Jeannin, P.Y., 2004. Temperature distribution in karst systems: the role of air and water fluxes. Terra Nova, 16, 344–350. https://doi.org/10.1111/j.1365-3121.2004.00572.x

Massei, N., Wang, H.Q., Field, M.S., Dupont, J.P., Bakalowicz, M., Rodet, J., 2006. Interpreting tracer breakthrough tailing in a conduit-dominated karstic aquifer. Hydrogeology Journal, 14, 849–858. https://doi.org/10.1007/s10040-005-0010-3

Moody, L.F., 1944. Friction factors for pipe flow. Transactions of American Society Mechanical Engineers, 66, 671–678. https://doi.org/10.1115/1.4018140

Palmer, A.N., Palmer, M.V., Sasowsky, I.D. (Eds.), 1999. Karst modeling. Proceedings of the symposium held in Februrary 24-27, 1999, Charlottesville, Virginia. Karst Water Institute, Special Publication 5, 265 p.

Pashchenko, A., Dublyansky, Y., Andreichuk, V., 1993. Aerosol study in the Kungur Ice Cave (Urals, Russia). Proceedings of the 11th International Congress of Speleology, Beijing 1, 190–192.

Pastore, C., Sedaghatkish, A., Schmid, N., Weber, E., Luetscher, M., 2024. Monitoring air fluxes in caves using digital flow metres. International Journal of Speleology, *in review*.

Piccini, L., 2011. Recent developments on morphometric analysis of karst caves. Acta Carsologica, 40(1), 43–52. https://doi.org/10.3986/ac.v40i1.27

Sasaki, K., Widiatmojo, A., Arpa, G., Sugai, Y., 2009. Airflow measurements and evaluation of effective diffusion coefficient in large scale of mine ventilation network using with tracer gas method. Journal of MMIJ, 125, 614–620. https://doi.org/10.2473/journalofmmij.125.614

Sauro, F., Pozzobon, R., Massironi, M., De Berardinis, P., Santagata, T., De Waele, J., 2020. Lava tubes on Earth, Moon and Mars: a review on their size and morphology revealed by comparative planetology. Earth-Science Reviews, 209, 103288. https://doi.org/10.1016/j.earscirev.2020.103288

Sauro, F., Zampieri, D., Filipponi, M., 2013. Development of a deep karst system within a transpressional structure of the Dolomites in north-east Italy. Geomorphology, 184, 51–63.
https://doi.org/10.1016/j.geomorph.2012.11.014

Semin, M.A., Isaevich, A.G., Trushkova, N.A., Bublik, S.A., Kazakov, B.P., 2022. Calculating dispersion of air pollutants in mines. Journal of Mining Science, 58, 246–256.
https://doi.org/10.1134/S1062739122020089

Standish, P.N., 1988. Dispersion mechanics in underground mine ventilation. Unpublished PhD Thesis, Department of Civil and Mining Engineering, University of Wollongong, Wollongong, 171 p.

Taylor, G., 1954. The dispersion of matter in turbulent flow through a pipe. Proceedings of the Royal Society, A 223, 446–468.
https://doi.org/10.1098/rspa.1954.0130

Thirnonsl, E.D., Kissel, F.N., 1974. Tracer gas as an aid in mine ventilation analysis. Bureau of Mines Report of Investigations, RI 7917, US Department of Interior, 17 p.

Widiatmojo, A., Sasaki, K., Sugai, Y., Suzuki, Y., Tanaka, H., Uchida, K., Matsumoto, H., 2015. Assessment of air dispersion characteristic in underground mine ventilation: Field measurement and numerical evaluation. Process Safety and Environmental Protection, 93, 173–181.
https://doi.org/10.1016/j.psep.2014.04.001

Widodo, N.P., Sasaki, K., Gautama, R.S., Risono, 2008. Mine ventilation measurements with tracer gas method and evaluations of turbulent diffusion coefficient. International Journal of Mining, Reclamation and Environment, 22, 60–69.
https://doi.org/10.1080/17480930701474869